Real Time Simulation of Multizone Elastokinematic Models

Doug L. James, Dinesh K. Pai
Dept. of Computer Science
University of British Columbia, Vancouver, Canada
E-mail: {djames|pai}@cs.ubc.ca

Abstract—
We introduce precomputed multizone elastokinematic models for interactive simulation of multibody kinematic systems which include elastostatic deformations. This enables an efficient form of domain decomposition, suitable for interactive simulation of stiff flexible structures for real time applications such as interactive assembly. One advantage of multizone models is that each zone can have small strains, and hence be modeled with linear elasticity, while the entire multizone/multibody system admits large nonlinear relative strains. This permits fast capacitance matrix algorithms and precomputed Green's functions to be used for efficient real time simulation. Examples are given for a human finger modeled as a kinematic chain with a compliant elastic covering.

Keywords— **Deformable objects, multibody simulation, haptics, force feedback, Green's functions, animation.**

I. Introduction and Related Work

PHYSICAL models used for real time simulation in robotics have been either rigid kinematic chains (e.g., almost all models of robot manipulators), dynamic flexible link models [1], or for a single deformable object (e.g., a liver [2]) possibly with a small inhomogeneous region of interest [3]. In this paper we generalize multibody kinematic systems to include linear elastostatic effects. These are important in many robotic applications involving nearly rigid elastic bodies [4]. Our method is even more general, in that it applies equally well to elastic objects that can be partitioned into connected regions or zones; hence we describe these as multizone elastokinematic models. They can also be used for rapid approximation of the global deformation due to contact between two or more elastic bodies, chains, or mechanisms (see also [5], which models the local compliance, but not global effects).

There has been significant work on interactive deformable objects recently [6], [7], [8], [9], [10], [2], [11]. Our approach exploits recently developed *capacitance matrix algorithms* for interactive simulation of linear elastostatic objects [7], [12], [11] (see also [8], [13]). High speed is obtained by precomputing discrete *Green's functions* [14] of the model, which intuitively provide a basis for describing all possible deformations of the object. Green's functions are extremely well suited for interaction with haptic interfaces [12] and can be directly estimated using robotic measurement [15]. This paper explores the fact that precomputed Green's functions also enable a very fast method for multizone condensation [16].

The rest of the paper is organized as follows. Section II summarizes necessary background on linear elastostatic Green's function models (LEGFMs), and section III motivates elastokinematic models. Section IV provides notation for describing multizone models, followed by a discussion of the simple case of contact between two objects defined in a common coordinate frame (in §V). The general case of a kinematic chain of bonded zones is discussed in §VI, with solution approaches described in §VII. Finally some results are provided in section VIII for a kinematic chain with a compliant elastic covering.

II. Background: Linear Elastostatic Green's Function Models (LEGFMs)

A. Displacement and Traction Boundary Values

We will describe discrete 3D elastic objects, e.g., finite element models, by their boundary values at "nodes." For concreteness, we assume that the surface displacement and traction fields are parametrized by N-vectors of nodal variables,

$$\mathsf{u} = [\mathsf{u}_1, \ldots, \mathsf{u}_N]^\mathsf{T} \quad (1)$$

$$\mathsf{p} = [\mathsf{p}_1, \ldots, \mathsf{p}_N]^\mathsf{T}, \quad (2)$$

where each of the N values, u_k and p_k, belong to $\mathbb{R}^3$. For example, our boundary element implementation uses vertex-based triangle mesh models in which nodes correspond to mesh vertices, and u_k and p_k describe the vertex displacement and traction, respectively, at the k^{th} vertex.

B. Reference Boundary Value Problem (RBVP)

A major benefit of using linear elastostatic models for real time simulation is that it is possible to precompute the Green's functions to one particular class

of boundary value problem (BVP), a relevant *reference BVP* (RBVP), and be able to efficiently compute components of those solutions rapidly at run time (see Figure 1).

Without loss of generality, assume that either position or traction constraints are specified at each boundary node. Let the mutually exclusive nodal index sets Λ_u^0 and Λ_p^0 specify nodes with displacement and traction constraints, respectively, so that $\Lambda_u^0 \cap \Lambda_p^0 = \emptyset$ and $\Lambda_u^0 \cup \Lambda_p^0 = \{1, 2, ..., N\}$. Specifying boundary values at each of the N nodes defines a BVP to be solved for desired unknown variables, e.g., resulting contact forces, at each step of the simulation. Denote the unspecified and complementary specified nodal variables by

$$\mathsf{v}_j = \begin{cases} \mathsf{p}_j & : \quad j \in \Lambda_u^0 \\ \mathsf{u}_j & : \quad j \in \Lambda_p^0 \end{cases} \quad \text{and} \quad \bar{\mathsf{v}}_j = \begin{cases} \bar{\mathsf{u}}_j & : \quad j \in \Lambda_u^0 \\ \bar{\mathsf{p}}_j & : \quad j \in \Lambda_p^0 \end{cases}$$

respectively.

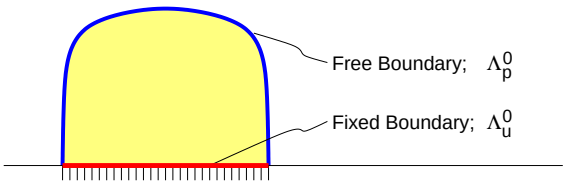

Fig. 1. *Reference Boundary Value Problem (RBVP) Example:* The RBVP associated with a model attached to a rigid support is shown with boundary regions indicated for nodes with displacement ("fixed," Λ_u^0) or traction ("free," Λ_p^0) constraints.

C. RBVP Solution using Green's Functions

The general solution of the RBVP is conveniently expressed in terms of the Green's functions (GFs) of the RBVP as

$$\mathsf{v} = \Xi \bar{\mathsf{v}} = \sum_{j \in \Lambda_u^0} \xi_j \bar{\mathsf{u}}_j + \sum_{j \in \Lambda_p^0} \xi_j \bar{\mathsf{p}}_j, \tag{3}$$

where the GFs are the block columns of the dense matrix

$$\Xi = [\xi_1 \xi_2 \cdots \xi_N] \in \mathbb{R}^{3N \times 3N}. \tag{4}$$

For example, the j^{th} GF, ξ_j describes the effect of the j^{th} node's specified boundary value, $\bar{\mathsf{v}}_j$, on the resulting solution. The benefit of the GF description is that once the GFs are known, the RBVP solution is given by a single matrix-vector multiplication. Precomputation of GFs for a particular RBVP type is possible since they only depend on the geometric and material properties of the deformable object. In practice it is only necessary to precompute GFs for nodes which have nonzero boundary values during the simulation.

The GF-based linear system description is possible for any discrete linear elastostatic model, regardless of internal material properties or the discretization technique employed. A detailed description of GF models and related *capacitance matrix algorithms* for simulation are presented in [11].

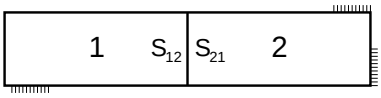

Fig. 2. *Two zone model* with zones and interface node sets indicated.

III. Multizone Kinematic Green's Function Models

Multizone models refer to objects comprised or several submodels, or "zones", connected by some physical constraints, e.g., see Figure 2. This type of domain decomposition is useful because (1) certain models are easily described or constructed using separate components, (2) it can reduce precomputation and storage costs for boundary descriptions, (3) it permits simulation of flexible kinematic structures, and (4) it approximates nonlinear strain in structures composed of precomputed linear substructures.

Multizone substructuring methods are commonly used in boundary element analysis, e.g., [16], to avoid the construction of large dense boundary element matrices for use with direct and iterative solvers. A common strategy is to use condensation on the system of multizone equations to arrive at a reduced system of equations relating only boundary values belonging to interzonal interfaces. Once these smaller condensed systems are solved, the interface values are then used to construct the solution on each domain.

By precomputing GFs for each zonal LEGFM, the condensed multizone matrix system can effectively be obtained "for free" from the GF lookup tables. The solution to the condensed interface equations is then used to determine the deformation of each zonal model using the capacitance matrix algorithm [12]. In this way, it is possible to interactively simulate large coupled systems.

IV. Multizone Model Notation

For the simple two zone model illustrated in Figure 2 consisting of zones 1 and 2, let the quantities associated with each LEGFM zone be denoted by a superscript 1 or 2. For example, the GFs of each zone are Ξ^1 and Ξ^2, the traction fields are p^1 and p^2, and displacements are u^1 and u^2, respectively. Initially, all quantities will be defined in a common coordinate system, but this will be generalized in §VI for more general kinematic relationships.

Let the interface between the zones be defined by two ordered lists of nodes: let S_{12} denote nodes in

zone 1 interfacing with zone 2, and similarly let S_{21} represent nodes in zone 2 contacting zone 1. Without loss of generality, we shall assume that the interface discretizations conform, so that the interface lists are the same size ($|\mathsf{S}_{12}| = |\mathsf{S}_{21}|$), and that the j^{th} node of each list corresponds to the same interface vertex. The interface displacements and tractions for zone 1 are then the arrays $\mathsf{u}^1_{\mathsf{S}_{12}}$ and $\mathsf{p}^1_{\mathsf{S}_{12}}$, while for zone 2 they are $\mathsf{u}^2_{\mathsf{S}_{21}}$ and $\mathsf{p}^2_{\mathsf{S}_{21}}$. For example, the subscript $()_{\mathsf{S}}$ implies that only components indices in S are contained in the subvector; this ordered list subscript notation is used throughout to specify submatrices.

V. Condensed Multizone Interface Equations

As a motivating example, consider the two-zone model shown in Figure 2 consisting of two models joined along a seam comprised of nodes with displacement boundary conditions in each model's reference BVP, i.e., seam nodes in Λ^0_u for each system. Note that it is equally easy to consider traction reference BVP conditions [11].

From (3), the interface tractions and displacements are related by

$$\mathsf{p}^1_{\mathsf{S}_{12}} = \hat{\mathsf{p}}^1_{\mathsf{S}_{12}} + \Xi^1_{\mathsf{S}_{12}\mathsf{S}_{12}} \mathsf{u}^1_{\mathsf{S}_{12}} \quad (5)$$

$$\mathsf{p}^2_{\mathsf{S}_{21}} = \hat{\mathsf{p}}^2_{\mathsf{S}_{21}} + \Xi^2_{\mathsf{S}_{21}\mathsf{S}_{21}} \mathsf{u}^2_{\mathsf{S}_{21}} \quad (6)$$

where the interfaces' self-influence matrices are square submatrices of Ξ, namely $\Xi^1_{\mathsf{S}_{12}\mathsf{S}_{12}}$ and $\Xi^2_{\mathsf{S}_{21}\mathsf{S}_{21}}$, and $\hat{\mathsf{p}}^1_{\mathsf{S}_{12}}$ and $\hat{\mathsf{p}}^2_{\mathsf{S}_{21}}$ describe the seam's traction contribution due to constraints outside the seam, e.g., a zone 1 nonzero traction constraint $\mathsf{p}^1_{j_1}$ at node $j_1 \in \Lambda^0_p$ (and therefore $j_1 \notin \mathsf{S}_{12}$) would imply

$$\hat{\mathsf{p}}^1_{\mathsf{S}_{12}} = \left(\xi^1_{j_1} \mathsf{p}^1_{j_1}\right)_{\mathsf{S}_{12}}. \quad (7)$$

The benefit of the multizone approach when combined with LEGFMs is immediately apparent from (5) and (6): condensed interface equations are available practically "for free" when given the precomputed GFs. This is a major benefit for real time, e.g., force feedback, applications since the global equilibrium can be determined by (direct) solution of small matrix problems involving only interface variables.

In order to physically bond the zonal LEGFMs at the interface, one may use the interface boundary conditions

$$\mathsf{u}^1_{\mathsf{S}_{12}} = +\mathsf{u}^2_{\mathsf{S}_{21}} \quad \text{(Continuity condition)} \quad (8)$$

$$\mathsf{p}^1_{\mathsf{S}_{12}} = -\mathsf{p}^2_{\mathsf{S}_{21}} \quad \text{(Newton's } 3^{rd} \text{ law)}. \quad (9)$$

Substituting these conditions into (5) and (6) and simplifying yields the linear system describing the interface constraints of the bonded material:

$$0 = \left(\Xi^1_{\mathsf{S}_{12}\mathsf{S}_{12}} + \Xi^2_{\mathsf{S}_{21}\mathsf{S}_{21}}\right) \mathsf{u}^2_{\mathsf{S}_{21}} + \hat{\mathsf{p}}^1_{\mathsf{S}_{12}} + \hat{\mathsf{p}}^2_{\mathsf{S}_{21}}. \quad (10)$$

Once the nonzero interface constraints are determined from this condensed interface equation they are applied to the LEGFMs in the usual way (using (3)) to compute the visual deformation.

VI. Elastokinematic Chains

In many ways, LEGFMs should be thought of as nearly rigid objects with an inherent frame of reference. Attaching the elastostatic model to a kinematic structure, such as a rigid frame or other support, is a natural way to associate this relationship in a simulation. By connecting together LEGFMs with multiple frames of reference, much larger relative deformations can be achieved than would otherwise be possible with a single LEGFM attached to multiple moving supports. While LEGFMs' linear Cauchy strain approximation of Green strain is not invariant under rotation, it is quite possible to rotate LEGFMs relative to each other. As an example, later in §VIII we shall consider animation of finger pad deformation during interactive grasping and contact tasks with a simplified finger model.

In this section, we shall consider a multizone kinematic chain of coupled LEGFMs as schematically shown in Figure 3. This multizone configuration results in a block tridiagonal system of equations comprising a nonlinear compliance equation relating the interface displacements (each defined in their LEGFM's frame of reference). These equations can then be efficiently solved in time linear in the number of zones. This is reminiscent of algorithms for linear time forward dynamics which have been shown to be equivalent to solving a (different) block tridiagonal system [17]. The stiffness response is nonlinear in the sense that it depends on the configuration of the joints in the chain, but for any single configuration it is linear.

We will describe kinematic chains only for notational simplicity, but the same arguments apply to other multizone interface topologies and kinematic structures. In practice the block sparse system of elastokinematic seam equations may cease to be block tridiagonal, but can still be efficiently solved [18], [16]. Issues related to kinematics, and means of handling them, are similar to those in rigid multibody dynamics [19], [20], [21], [22].

Similar boundary influence equations for coupling elastic bodies in equilibrium arise when computing contact constraints between multiple elastic objects [23], [24]. Using the precomputed GF models, the contact response could be efficiently computed and integrated at high rates to solve simplified contact problems interactively, e.g., with haptic force feedback.

The LEGFM's zonal frames of reference are related

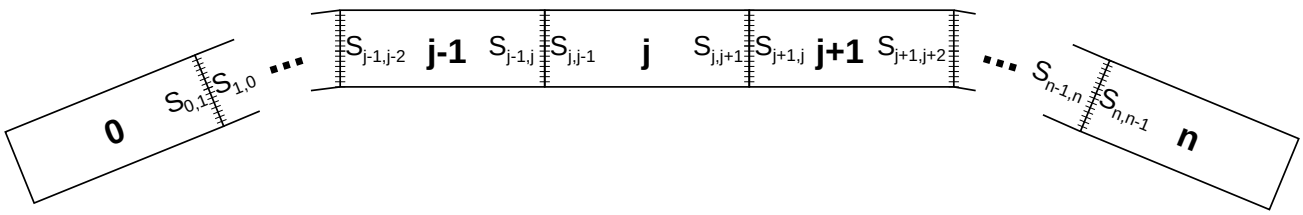

Fig. 3. *Multizone elastokinematic chain model schematic* with zones and interface node sets indicated. Here interface nodes have displacement constraints in each zone's RBVP, and external constraints are not shown.

by coordinate transformations: let the operator ${}^{j}_{j+1}\mathsf{F}$ map quantities from frame $j+1$ to j, and ${}^{j+1}_{j}\mathsf{F}$ from j to $j+1$. A left superscript will denote the frame of reference of a quantity, e.g., ${}^{j}a^{i}$ represents a quantity a of zone i in frame of zone j. Some illustrative coordinate transformations of quantities in zone j from frame j to $j+1$ are

$$
\begin{aligned}
{}^{j+1}\mathsf{u}^{j}_{\mathsf{S}} &= {}^{j+1}_{j}\mathsf{F}\,{}^{j}\mathsf{u}^{j}_{\mathsf{S}} && (11)\\
{}^{j+1}\Xi^{j}_{\mathsf{SS}} &= {}^{j+1}_{j}\mathsf{F}\,{}^{j}\Xi^{j}_{\mathsf{SS}}. && (12)
\end{aligned}
$$

Taking the RBVP of each zone to have specified displacement boundary conditions for seam constraints (see Figure 3), the LEGFM equations describing the traction response on both sides (j and $j+1$) of seam $j = 0, 1, \ldots, n-1$ are

$$
\begin{aligned}
{}^{j}\mathsf{p}^{j}_{\mathsf{S}_{j,j+1}} &= {}^{j}\hat{\mathsf{p}}^{j}_{\mathsf{S}_{j,j+1}} + {}^{j}\Xi^{j}_{\mathsf{S}_{j,j+1}\mathsf{S}_{j,j+1}}\,{}^{j}\mathsf{u}^{j}_{\mathsf{S}_{j,j+1}}\\
&\quad + {}^{j}\Xi^{j}_{\mathsf{S}_{j,j+1}\mathsf{S}_{j,j-1}}\,{}^{j}\mathsf{u}^{j}_{\mathsf{S}_{j,j-1}}\\
{}^{j+1}\mathsf{p}^{j+1}_{\mathsf{S}_{j+1,j}} &= {}^{j+1}\hat{\mathsf{p}}^{j+1}_{\mathsf{S}_{j+1,j}} + {}^{j+1}\Xi^{j+1}_{\mathsf{S}_{j+1,j}\mathsf{S}_{j+1,j}}\,{}^{j+1}\mathsf{u}^{j+1}_{\mathsf{S}_{j+1,j}}\\
&\quad + {}^{j+1}\Xi^{j+1}_{\mathsf{S}_{j+1,j}\mathsf{S}_{j+1,j+2}}\,{}^{j+1}\mathsf{u}^{j+1}_{\mathsf{S}_{j+1,j+2}}
\end{aligned}
$$

where the node sets $\mathsf{S}_{0,-1}$ and $\mathsf{S}_{n,n+1}$ may be taken as the empty set to yield the end seam equations

$$
\begin{aligned}
{}^{0}\mathsf{p}^{0}_{\mathsf{S}_{01}} &= {}^{0}\hat{\mathsf{p}}^{0}_{\mathsf{S}_{01}} + {}^{0}\Xi^{0}_{\mathsf{S}_{01}\mathsf{S}_{01}}\,{}^{0}\mathsf{u}^{0}_{\mathsf{S}_{01}}\\
{}^{n}\mathsf{p}^{n}_{\mathsf{S}_{n,n-1}} &= {}^{n}\hat{\mathsf{p}}^{n}_{\mathsf{S}_{n,n-1}} + {}^{n}\Xi^{n}_{\mathsf{S}_{n,n-1}\mathsf{S}_{n,n-1}}\,{}^{n}\mathsf{u}^{n}_{\mathsf{S}_{n,n-1}}.
\end{aligned}
$$

The seam bonding conditions, respectively similar to (8) and (9), but accounting for transformations between zone frames of reference, are

$$
\begin{aligned}
{}^{j}\mathsf{x}^{j}_{\mathsf{S}_{j,j+1}} + {}^{j}\mathsf{u}^{j}_{\mathsf{S}_{j,j+1}} &= {}^{j}_{j+1}\mathsf{F}\left({}^{j+1}\mathsf{x}^{j+1}_{\mathsf{S}_{j+1,j}} + {}^{j+1}\mathsf{u}^{j+1}_{\mathsf{S}_{j+1,j}}\right)\\
0 &= {}^{j}\mathsf{p}^{j}_{\mathsf{S}_{j,j+1}} + {}^{j}_{j+1}\mathsf{F}\,{}^{j+1}\mathsf{p}^{j+1}_{\mathsf{S}_{j+1,j}}
\end{aligned}
$$

where ${}^{j}\mathsf{x}^{j}_{*}$ represent undisplaced vertex positions. These seam conditions may be rewritten for substitution as

$$
\begin{aligned}
{}^{j+1}\mathsf{u}^{j+1}_{\mathsf{S}_{j+1,j}} &= {}^{j+1}_{j}\mathsf{F}\left({}^{j}\mathsf{x}^{j}_{\mathsf{S}_{j,j+1}} + {}^{j}\mathsf{u}^{j}_{\mathsf{S}_{j,j+1}}\right) - {}^{j+1}\mathsf{x}^{j+1}_{\mathsf{S}_{j+1,j}}\\
{}^{j+1}\mathsf{p}^{j+1}_{\mathsf{S}_{j+1,j}} &= -{}^{j+1}_{j}\mathsf{F}\,{}^{j}\mathsf{p}^{j}_{\mathsf{S}_{j,j+1}}.
\end{aligned}
$$

Substituting the bonding conditions into the LEGFM equations by eliminating variables with non-increasing interface index pairs[1] we obtain the nonsymmetric block tridiagonal elastokinematic chain's seam equations relating each set of seam displacements (each in its natural frame of reference) to adjacent seams:

$$
\begin{aligned}
0 &= \left({}^{j}\Xi^{j}_{\mathsf{S}_{j,j+1}\mathsf{S}_{j,j-1}}\,{}^{j}_{j-1}\mathsf{F}\right){}^{j-1}\mathsf{u}^{j-1}_{\mathsf{S}_{j-1,j}}\\
&\quad + \left({}^{j}\Xi^{j}_{\mathsf{S}_{j,j+1}\mathsf{S}_{j,j+1}} + {}^{j}\Xi^{j+1}_{\mathsf{S}_{j+1,j}\mathsf{S}_{j+1,j}}\,{}^{j+1}_{j}\mathsf{F}\right){}^{j}\mathsf{u}^{j}_{\mathsf{S}_{j,j+1}}\\
&\quad + \left({}^{j}\Xi^{j+1}_{\mathsf{S}_{j+1,j}\mathsf{S}_{j+1,j+2}}\right){}^{j+1}\mathsf{u}^{j+1}_{\mathsf{S}_{j+1,j+2}}\\
&\quad + {}^{j}\hat{\mathsf{p}}^{j}_{\mathsf{S}_{j,j+1}} + {}^{j}\hat{\mathsf{p}}^{j+1}_{\mathsf{S}_{j+1,j}} \qquad (13)\\
&\quad + {}^{j}\Xi^{j}_{\mathsf{S}_{j,j+1}\mathsf{S}_{j,j-1}}\left({}^{j}\mathsf{x}^{j-1}_{\mathsf{S}_{j-1,j}} - {}^{j}\mathsf{x}^{j}_{\mathsf{S}_{j,j-1}}\right)\\
&\quad + {}^{j}\Xi^{j+1}_{\mathsf{S}_{j+1,j}\mathsf{S}_{j+1,j}}\left({}^{j+1}\mathsf{x}^{j}_{\mathsf{S}_{j,j+1}} - {}^{j+1}\mathsf{x}^{j+1}_{\mathsf{S}_{j+1,j}}\right)
\end{aligned}
$$

for $j = 0, 1, \ldots, n-1$ and $\mathsf{S}_{0,-1} = \mathsf{S}_{n,n+1} = \emptyset$. Note that this is the elastokinematic chain generalization of (10) for the two zone model.

VII. Solution of Elastokinematic BVP

The elastokinematic equations exhibit nonlinear dependence on chain orientation, but for any single orientation they are linear; given $\{{}^{j+1}_{j}\mathsf{F}\}$ the linear matrix system may be efficiently solved in several ways.

A suitable direct approach is to use block tridiagonal LU factorization methods [18], which are effective given the condensed interface equations and small sets of interface variables. As mentioned earlier, the cost of this approach is linear in the number of zones. The factorization must be performed for each different chain orientation, but suitable interpolation can be used.

Iterative solution methods are another well-established tool for solving multizone equations and especially their condensed variants (see [16]; note that condensation costs are precomputed here). However, their solution costs can be less predictable than direct solvers. Nevertheless, good preconditioners can be constructed by observing the matrix properties; the block tridiagonal equations often have very dominant diagonal blocks so that a good preconditioner can be

[1] For example, eliminate $\mathsf{u}_{\mathsf{S}_{j+1,j}}$ but keep $\mathsf{u}_{\mathsf{S}_{j,j+1}}$.

constructed using their LU factorizations. For example, the finger model presented in §VIII has diagonal elements which are more than 100 times more significant than the off diagonal elements, and therefore convergence is rapid.

There are further means for accelerating this process. Probably the most systematic and effective approach to reducing the number of seam variables is to use multiresolution constraint descriptions [11]. For models with weakly coupled seams, such as the finger example, an approximation is to let the system matrix be block diagonal; the diagonal blocks can even be factorized for a small number of joint angles and interpolated. Another approximation is to only constrain seam degrees of freedom near the surface.

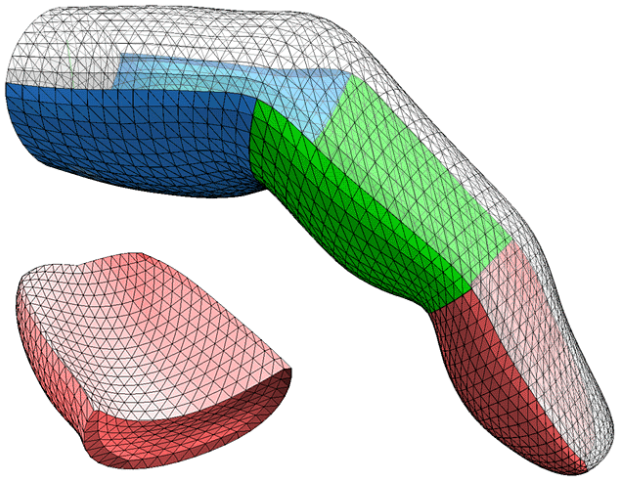

Fig. 4. *Finger model with three individual elastostatic finger pads:* The distal bone's fingertip pad (1664 triangles and 834 vertices) is drawn inset for clarity. Green's functions are precomputed for each finger pad, and the models are connected by continuity constraints.

VIII. Example: Compliant Skin on a Rigid Kinematic Chain

We have implemented a multizone model for real time simulation of a finger (Figures 4–7). Such a model could be used to simulate a robotic hand with a compliant skin covering the finger and joints, or for interactive computer animation of a human hand. Precomputed multiresolution LEGFMs [11] (computed with boundary element analysis) are used for each finger pad, with displacement constraints specified at "bone" and seam vertices of each zone's RBVP. The finger pads are connected by continuity constraints at interface seams located near kinematic joints. The resulting nonlinear elastokinematic equations (13) approximate the nonlinear strains associated with finger bending motions.

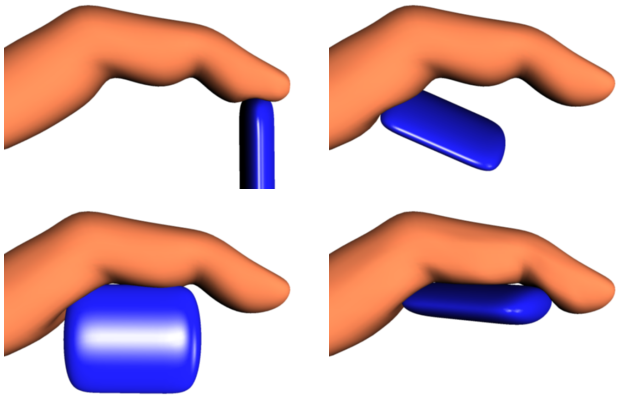

Fig. 5. *Interactive simulation of contact* between the elastokinematic finger and a rigid manipulandum.

For real time animation applications with very low computing budgets, such as video games, a precomputed block diagonal approximation of (13) could be used. A more dramatic approximation, which decouples zones and avoids the solution of the elastokinematic equation, is achieved by specifying interface position constraints kinematically using, e.g., Skeletal Subspace Deformation [25]. As the kinematic joints move, the displacement constraints applied in each LEGFM's frame of reference also change. In this manner, incorporating LEGFMs into skeletal animations is relatively straight-forward.

The elastokinematic finger model was simulated in our Java-based ArtDefo simulator [7]. Simulation screenshots are shown for unilateral contact simulation running at video rates (Figure 5), force feedback rendering of point-like contact at 1 kHz (Figure 6), and skeleton-driven finger motions (Figure 7). We note that several performance improvements are possible using multiresolution enhancements detailed in [11].

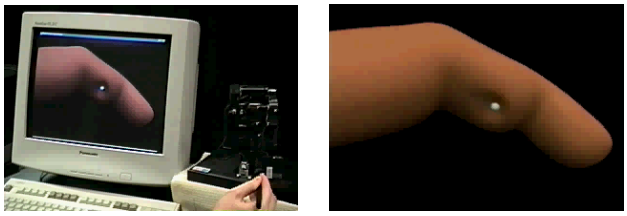

Fig. 6. *Force feedback rendering* of point-like contact using a PHANTOM Premium 1.0 device.

IX. Summary

We have introduced a multizone elastokinematic model formulation based on the coupling of precomputed linear elastostatic Green's function models. The approach has proven suitable for real time interactive

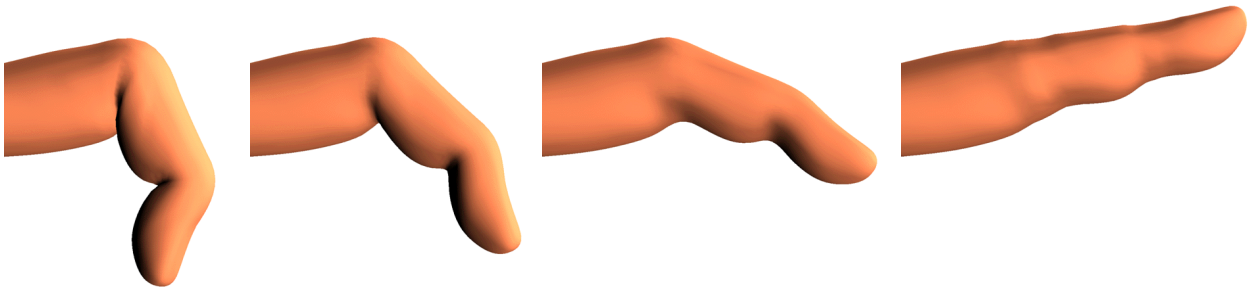

Fig. 7. *Simulation of finger with elastic finger pads:* An illustrative skeleton-driven animation of a deformable finger modeled using three individual linear elastostatic finger pads. Each finger pad is defined in a frame of reference rigidly attached to its corresponding "bone," thus allowing large relative strains to be simulated as the skeleton moves. Vertices not on finger pads are geometrically deformed and so do not deform under contact.

applications, and has been demonstrated for the case of a kinematic chain with a compliant covering.

References

[1] Inna Sharf and Gabriele M.T. D'Eleuterio, "Parallel Simulation Dynamics for Elastic Multibody Chains," *IEEE Transactions on Robotics and Automation*, vol. 8, no. 5, October 1992.

[2] G. Picinbono, H. Delingette, and N. Ayache, "Non-linear and Anisotropic Elastic Soft Tissue Models for Medical Simulation," in *ICRA2001: IEEE International Conference on Robotics and Automation*, Seoul Korea, May 2001.

[3] K. V. Hansen and O. V. Larsen, "Using Region-of-Interest Based Finite Element Modeling for Brain-Surgery Simulation," *Lecture Notes in Computer Science*, vol. 1496, pp. 305–, 1998.

[4] F. Xi and R.G. Fenton, "Point-To-Point Quasi-Static Motion Planning for Flexible-Link Manipulators," *IEEE Transactions on Robotics and Automation*, vol. 11, no. 5, October 1995.

[5] P. Song, P. Kraus, V. Kumar, and P. Dupont, "Analysis of Rigid Body Dynamic Models for Simulation of Systems with Frictional Contacts," *ASME Transactions Journal of Applied Mechanics*, pp. 118–128, 2001.

[6] Sarah F. Gibson and Brian Mirtich, "A Survey of Deformable Models in Computer Graphics," Tech. Rep. TR-97-19, Mitsubishi Electric Research Laboratories, Cambridge, MA, November 1997.

[7] Doug L. James and Dinesh K. Pai, "ArtDefo: Accurate Real Time Deformable Objects," *Computer Graphics*, vol. 33, no. Annual Conference Series, pp. 65–72, 1999.

[8] S. Cotin, H. Delingette, and N. Ayache, "Realtime Elastic Deformations of Soft Tissues for Surgery Simulation," *IEEE Transactions On Visualization and Computer Graphics*, vol. 5, no. 1, pp. 62–73, 1999.

[9] Yan Zhuang and John Canny, "Haptic Interaction with Global Deformations," in *Proceedings of the IEEE International Conference on Robotics and Automation*, 2000.

[10] Gilles Debunne, Mathieu Desbrun, Alan Barr, and Marie-Paule Cani, "Dynamic Real-Time Deformations Using Space and Time Adaptive Sampling," in *Computer Graphics (SIGGRAPH 2001 Proceedings)*, 2001.

[11] Doug L. James, *Multiresolution Green's Function Methods for Interactive Simulation of Large-scale Elastostatic Objects and Other Physical Systems in Equilibrium*, Ph.D. thesis, Institute of Applied Mathematics, University of British Columbia, Vancouver, British Columbia, Canada, 2001.

[12] Doug L. James and Dinesh K. Pai, "A Unified Treatment of Elastostatic Contact Simulation for Real Time Haptics," *Haptics-e, The Electronic Journal of Haptics Research (www.haptics-e.org)*, vol. 2, no. 1, September 2001.

[13] J. Berkley, S. Weghorst, H. Gladstone, G. Raugi, D. Berg, and M. Ganter, "Fast Finite Element Modeling for Surgical Simulation," in *Proceedings of Medicine Meets Virtual Reality*, 1999, pp. 55–61.

[14] Dean G. Duffy, *Green's Functions with Applications*, Chapman & Hall, Boca Raton, Florida, 2001.

[15] Dinesh K. Pai, Kees van den Doel, Doug L. James, Jochen Lang, John E. Lloyd, Joshua L. Richmond, and Som H. Yau, "Scanning Physical Interaction Behavior of 3D Objects," in *Computer Graphics Proceedings (SIGGRAPH 2001)*. 2001, ACM Siggraph.

[16] J. H. Kane, D. E. Keyes, and K. Guru Prasad, "Iterative Solution Techniques in Boundary Element Analysis," *International Journal for Numerical Methods in Engineering*, vol. 31, pp. 1511–1536, 1991.

[17] D. K. Pai, U. M. Ascher, and P. G. Kry, "Forward Dynamics Algorithms for Multibody Chains and Contact," in *Proceedings of the 2000 IEEE International Conference on Robotics and Automation*, San Francisco, April 2000, pp. 857–863.

[18] Gene H. Golub and Charles F. Van Loan, *Matrix Computations*, Johns Hopkins University Press, Baltimore and London, third edition, 1996.

[19] U. Ascher, D. K. Pai, and B. Cloutier, "Forward Dynamics, Elimination Methods, and Formulation Stiffness in Robot Simulation," *International Journal of Robotics Research*, vol. 16, no. 6, pp. 749–758, December 1997.

[20] C. Lubich, U. Nowak, U. Pohle, and Ch. Engstler, "MEXX – Numerical software for the integration of constrained mechanical multibody systems," Tech. report SC92-12, Konrad-Zuse-Zentrum für Informationstechnik, Berlin., 1992.

[21] David Baraff, "Linear-Time Simulation using Lagrange Multipliers," in *SIGGRAPH 96 Conference Proceedings*, 1996, pp. 137–146.

[22] Roy Featherstone, *Robot Dynamics Algorithms*, Kluwer, 1987.

[23] Y. Ezawa and N. Okamoto, "High-speed Boundary Element Contact Stress Analysis using a Super Computer," in *Proc. of the* 4^{th} *International Conference on Boundary Element Technology*, 1989, pp. 405–416.

[24] K. W. Man, M. H. Aliabadi, and D. P. Rooke, "Analysis of Contact Friction using the Boundary Element Method," in *Computational Methods in Contact Mechanics*, M. H. Aliabadi and C. A. Brebbia, Eds., chapter 1, pp. 1–60. Computational Mechanics Publications and Elsevier Applied Science, 1993.

[25] N. Magnenat-Thalmann, R. Laperriere, and D. Thalmann, "Joint-Dependent Local Deformations for Hand Animation and Object Grasping," in *Proc. of Graphics Interface '88*, June 1988, pp. 26–33.